RSC Advances

PAPER

View Article Online
View Journal | View Issue

Check for updates

Cite this: *RSC Adv.*, 2021, **11**, 33309

A series of lanthanide–quinoxaline-2,3(1*H*,4*H*)-dione complexes containing 1D chiral Ln_2O_3 (Ln = Eu, Tb, Sm, Dy) chains: luminescent properties and response to small molecules†

Sadaf ul Hassan, *[abd] Muhammad Asim Farid[cd] and Yingxia Wang*[d]

Five new isostructural lanthanide–organic complexes, $[Ln_2O_2(OH)(HQXD)(H_2QXD)_2]\cdot H_2O$ (Ln = Eu **1**, Tb **2**, Sm **3** Dy **4** and Gd **5**; H_2QXD = quinoxaline-2,3(1*H*,4*H*)-dione), have been synthesized under hydrothermal conditions. These complexes are characterized by powder X-ray diffraction (PXRD), infrared spectroscopy (IR), elemental analysis (EA), thermogravimetric-differential thermal analysis (TG-DTA) and photo-luminescent spectroscopy. Single crystal X-ray diffraction analysis of complex **1** revealed that the structure featured in 1D chiral "Eu_2O_3" chains surrounded by coordinating organic ligands. These chains are interconnected *via* hydrogen bonding and offset π···π stacking interactions of the ligands to form the 3D supramolecular frameworks. The photo-luminescence studies for complexes **1–5** disclosed that the ligand (H_2QXD) showed an antenna effect to transfer energy toward the lanthanide cations. The energy transfer mechanism investigations show that the energy transition from the triplet energy level ($^3\pi\pi^*$) of ligand H_2QXD to the Tb^{3+} cation is more effective than to the Eu^{3+}, Sm^{3+} and Dy^{3+} ions; therefore it has been selected as a representative to examine the potential for sensing small molecules. Complex **2′**, which was obtained by the heating treatment of **2** at 150 °C, displayed a high luminescence sensitivity towards small solvent molecules. Tertiary butanol (*t*-butanol) was found to be an excellent sensitizer, while tetrahydrofuran (THF) was a highly quenching species. Complex **2′** could regain a higher photo-luminescence intensity after treating for 5 cycles with *t*-butanol, revealing a prospect for reusability.

Received 27th July 2021
Accepted 20th September 2021

DOI: 10.1039/d1ra05719g

rsc.li/rsc-advances

Open Access Article. Published on 29 October 2021. Downloaded on 1/21/2026 12:04:46 AM.
This article is licensed under a Creative Commons Attribution-NonCommercial 3.0 Unported Licence.

Introduction

Metal–Organic Framework (MOF) materials as chemical sensors have attracted considerable attention due to their intriguing topological structures as well as potential applications in recognition and luminescence based sensing of guest molecules.[1–4] Luminescence based sensing is typically a useful technique in many biological processes in which luminescence intensity is quenched or enhanced by the sensor to recognize the guest molecules.[5,6] However, the precise sensing of small guest molecules by using this technique is still ambiguous because the influence factors on the sensibility include not only the primary interactions such as coordination environment of metals, nature of the ligands and pore size of surfaces, but also the synergistic weak interactions caused by guest species *via* hydrogen bonding, van der Waals forces, π···π stacking, non-radioactive deactivation process and *etc.*[7–9] Though such kinds of weak interactions are more flexible than the coordination bonds therefore they can lead to the construction of 3D frameworks and may also influence the properties by inducing guest molecules.[10]

Recently, lanthanide metal–organic frameworks (Ln-MOFs) have been considered as promising luminescent sensing materials because they can generate the visible luminescence under UV light.[3,10,11] The Ln-MOFs constructed by lanthanide cations (Ln^{3+}) such as Eu^{3+} and Tb^{3+} are good choices to construct photo-luminescent systems due to their high coordination numbers and variable environments, especially they exhibit high color purity and fluorescent efficiency.[12] However the direct excitation of electron in the trivalent lanthanide ions is usually inefficient due to their poor absorption of UV-light from the Laporte forbidden f → f transitions.[13] Therefore, incorporation of suitable organic linkers/chromophores to gain and then transfer energy is demanded to increase the

[a]*University of Management & Technology, Lahore campus, Lahore, 54770, Pakistan*
[b]*COMSATS University Islamabad (CUI), Lahore Campus, Lahore, 54000, Pakistan. E-mail: sadaf.hassan@umt.edu.pk*
[c]*Department of Chemistry, Division of Science and Technology, University of Education, Lahore, Pakistan*
[d]*State Key Laboratory of Rare Earth Materials Chemistry and Applications, College of Chemistry and Molecular Engineering, Peking University, Beijing 100871, P. R. China. E-mail: yxwang@pku.edu.cn; Fax: +8610 6275; Tel: +8610 6275 5538*

† Electronic supplementary information (ESI) available. CCDC 1521675. For ESI and crystallographic data in CIF or other electronic format see DOI: 10.1039/d1ra05719g

© 2021 The Author(s). Published by the Royal Society of Chemistry

Open Access Article. Published on 29 October 2021. Downloaded on 1/21/2026 12:04:46 AM.
This article is licensed under a Creative Commons Attribution-NonCommercial 3.0 Unported Licence.

luminescent efficiency of Ln-MOFs to overcome the shortcomings of the low extinction coefficients of Ln^{3+} ions.[14]

Herein, we selected a stable, conjugated and rigid organic molecule, quinoxaline-2,3(1*H*,4*H*)-dione (H_2QXD), as ligand for antenna sensitization, and synthesized a new series of five isostructural lanthanide complexes $[Ln_2O_2(OH)(HQXD)(H_2QXD)_2]\cdot H_2O$ (Ln = Eu(III) **1**, Tb(III) **2**, Sm(III) **3** Dy(III) **4** and Gd(III) **5**) which featured in 3D supramolecular networks formed by 1D chiral "Ln_2O_3" chains *via* hydrogen bonding and offset $\pi\cdots\pi$ stacking of the ligands. The photo-luminescent properties of title complexes have been studied. Complex **2′**, which was obtained by the heating treatment of **2** at 150 °C, displayed high-sensitivity towards the small solvents molecules, wherein tertiary butanol (*t*-butanol) was found to be an excellent sensitizer and tetrahydrofuran (THF) was a highly quenching species. Complex **2′** regained almost 70% of its first photo-luminescent intensity, revealing a prospect for its reusability.

Experimental

Reagents and general techniques

All chemicals (*o*-pheylenediamine, oxalic acid dehydrate, lanthanide oxide (*i.e.*, Eu_2O_3, Tb_4O_7, Sm_2O_3, Dy_2O_3 and Gd_2O_3)) of reagent grade quality are obtained commercially and used without further purifications. Quinoxaline-2,3(1*H*,4*H*)-dione (H_2QXD) is prepared according to the reported method.[15] Elemental analyses for C, H, N were performed on a Perkin-Elmer 240C analytical instrument, while the analyses for Eu, Tb, Sm and Dy in solution by dissolving the samples in dilute hydrochloric acid were performed using an ICPS-7500 model inductively coupled plasma emission spectrometer (ICP-ES). Powder X-ray diffraction (PXRD) data were collected on a PANalytical X'Pert3 diffractometer with Cu Kα (1.5418 Å) radiation at 40 kV and 40 mA at room temperature. The powder X-ray diffraction data were analyzed using GSAS software to find the structural parameters.[16] Suitable colorless single crystal of **1** with the size of 0.111 × 0.029 × 0.018 mm^3 was carefully selected under an optical microscope. Then single crystal X-ray diffraction data was collected on an Agilent Supernova CCD diffractometer with Mo Kα radiation source (λ = 0.71073 Å) and graphite monochromator at 180 K. The structure was solved by direct method and refined with the SHELX 97 program package.[17] The final refinement was performed by full matrix least squares methods with anisotropic thermal parameters for non-hydrogen atoms on $|F|^2$.[18] Detailed crystallographic information is listed in Table 1. CIF file containing atomic coordinates is deposited in Cambridge Crystallographic Data Centre with the CCDC number of 1521675. Selected bond lengths, and angles are listed in ESI (Table S1†). FTIR (KBr pellets) spectra were recorded on a Magna-IR 750 spectrophotometer in 4000–400 cm^{-1} range. Thermo gravimetric analyses (TGA) and differential thermal analyses (DTA) were performed on a NETZSCH STA 449 C unit at a heating rate of 10 °C min^{-1} under argon. The UV-Vis, spectra were recorded on a Shimadzu UV-2550 spectrophotometer in the range of 200–800 nm. The phosphorescence spectrum of gadolinium-complex (Gd^{3+}complex) in the solid state at 77 K and photo-luminescence measurements of all complexes were recorded by using a Hitachi F-7000 FL fluorescence spectrophotometer with both excitation and emission slits of 5 nm, using a xenon arc lamp as the light source (150 W), the photomultiplier tube voltage was 400 V, the scan speed was 1200 nm min^{-1} and 350 nm filter was used. The luminescence decay curves and photoluminescence quantum yields of the samples were obtained using a FLS 980 combined fluorescence lifetime and a steady state spectrometer.

Hydrothermal synthesis of $[Ln_2O_2(OH)(HQXD)(H_2QXD)_2]\cdot H_2O$

The five complexes were obtained by hydrothermal reaction of a measured amount of lanthanide oxides, H_2QXD (0.065 g, 0.40 mmol) and 10 mL water in a 25 mL Teflon-lined autoclave at 170 °C for 3 days.

$[Eu_2O_2(OH)(HQXD)(H_2QXD)_2]\cdot H_2O$ (1). Colourless needle crystals. Its yield is 0.0134 g, about 13% based on Eu (Eu_2O_3: 0.042 g, 0.12 mmol). Anal. calcd for $C_{24}H_{20}N_6O_{10}Eu_2$: C, 33.66, H, 2.35, N, 9.81 wt%. Found: C, 33.63, H, 2.34, N, 9.80 wt%. IR (KBr ν/cm^{-1}): 2996 (w), 2916 (w), 2832 (w), 1628 (s), 1445 (m), 1327 (m), 804 (m), 696 (w), 583 (w) and 521 (w).

$[Tb_2O_2(OH)(HQXD)(H_2QXD)_2]\cdot H_2O$ (2). Colourless crystals. Its yield is 0.0125 g, about 12% based on Tb (Tb_4O_7: 0.046 g, 0.062 mmol). Anal. calcd for $C_{24}H_{20}N_6O_{10}Tb_2$: C, 33.12, H, 2.32, N, 9.66 wt%. Found: C, 33.12, H, 2.29, N, 9.65 wt%. IR (KBr ν/cm^{-1}): 3000 (w), 2917 (w), 2828 (w), 1624 (s), 1449 (m), 1325 (m), 800 (m), 695 (w), 582 (w) and 521 (w).

$[Sm_2O_2(OH)(HQXD)(H_2QXD)_2]\cdot H_2O$ (3). Yellow crystals. Yield: 0.0155 g, *ca.* 15% based on Sm (Sm_2O_3: 0.042 g, 0.12 mmol). Anal. calcd $C_{24}H_{20}N_6O_{10}Sm_2$: C, 33.79, H, 2.36, N, 9.85 wt%. Found: C, 33.72, H, 2.26, N, 9.79 wt%. IR (KBr ν/cm^{-1}): 2995 (w), 2911 (w), 2826 (w), 1631 (s), 1442 (m), 1321 (m), 802 (m), 700 (w), 577 (w) and 517 (w).

$[Dy_2O_2(OH)(HQXD)(H_2QXD)_2]\cdot H_2O$ (4). Light yellow needle crystals. Yield: 0.0152 g, *ca.* 14% based on Dy (Dy_2O_3: 0.045 g, 0.12 mmol). Anal. calcd for $C_{24}H_{20}N_6O_{10}Dy_2$: C, 32.85, H, 2.30, N, 9.58 wt%. Found: C, 32.82, H, 2.27, N, 9.52 wt%. IR (KBr ν/cm^{-1}): 2992 (w), 2909 (w), 2823 (w), 1629 (s), 1439 (m), 1331 (m), 792 (m), 706 (w), 572 (w) and 514 (w).

$[Gd_2O_2(OH)(HQXD)(H_2QXD)_2]\cdot H_2O$ (5). Light yellow needle crystals. Yield: 0.0139 g, *ca.* 13% based on Dy (Gd_2O_3: 0.045 g, 0.12 mmol). Anal. calcd for $C_{24}H_{20}N_6O_{10}Gd_2$: C, 33.25, H, 2.33, N, 9.69 wt%. Found: C, 33.12, H, 2.31, N, 9.62 wt%. IR (KBr ν/cm^{-1}): 2997 (w), 2903 (w), 2827 (w), 1633 (s), 1431 (m), 1335 (m), 790 (m), 701 (w), 578 (w) and 519 (w).

Results and discussion

Phase identification and refinement of lattice parameters

The powder X-ray diffraction patterns (PXRD) of H_2QXD ligand and complexes **1–5** at room temperature are shown in Fig. 1. The similar PXRD patterns of complexes **1–5** indicate that they may take the same structural fashion. No obvious peaks were found for impurities. The powder X-ray diffraction data complexes **1–5** are refined through Rietveld refinement method

© 2021 The Author(s). Published by the Royal Society of Chemistry

Open Access Article. Published on 29 October 2021. Downloaded on 1/21/2026 12:04:46 AM.
This article is licensed under a Creative Commons Attribution-NonCommercial 3.0 Unported Licence.

Table 1 Crystal data and structure refinement parameters for complex **1**

Item	Information	Item	Information
Empirical formula	$C_{24}H_{20}Eu_2N_6O_{10}$	Temp. (K)	180.0
Formula mass (g mol^{-1})	856.38	F(000)	1648
Crystal system	Monoclinic	Crystal size (mm^3)	0.111 × 0.029 × 0.018
		Morphology	Needle shaped
Space group	$P2_1/n$	Index ranges	$-8 \le h \le 8$; $-15 \le k \le 10$; $-30 \le l \le 30$
a (Å)	7.4220(3)	Number of reflections measured	9563
b (Å)	25.7340(1)	Number of independent reflections	4385
c (Å)	13.2847(8)	Number of observed reflections	3212
α (°)	90	Number of refined parameters	175
β (°)	100.008(5)	Independent reflections [R (int)]	0.0594
γ (°)	90	Data/restraints/parameters	4385/0/374
Volume (Å^3)	2498.799(2)	Goodness-of-fit on F^2	1.055
Z	4	Final R indices [$I > 2\sigma(I)$]	$R_1 = 0.0510$, w$R_2 = 0.0989$
Density (g cm^{-3})	2.276	R indices (all data)	$R_1 = 0.0845$, w$R_2 = 0.1133$
Absorption coefficient (mm^{-1})	5.048	Largest diff. peak and hole (e Å^{-3})	1.829 and −1.201
F(000)	1648	CCDC number	1521675

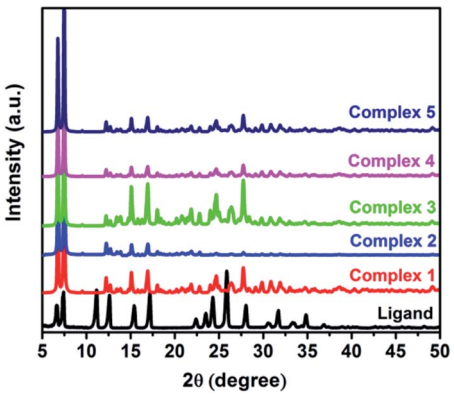

Fig. 1 Powder X-ray diffraction patterns of H_2QXD and complexes **1**–**5**.

with gsas software to get the cell parameters of each complex. The powder X-ray diffraction data is refined using the structural parameters obtained from the single crystal X-ray diffraction analysis for complex **1** (Table 1). Good refinement results are obtained with refinement factors Rwp$^x \le 0.025$ and Rp$^x \le 0.013$. The typical Rietveld plots of powder X-ray diffraction data of complexes **1**–**5** are shown in Fig. S1 in ESI.† The lattice parameters are listed in Table 2, and the change of the parameters is normal, which is consistent with the change of the radii of the lanthanide cations in eight coordinate. The refined results confirm that the complexes **1**–**5** are isostructural and crystallize in triclinic structure with $P2_1/n$ space group. Therefore, the structure of complex **1** determined by the single crystal X-ray diffraction data is discussed in detail as the representative.

The refined results confirm that the complexes **1**–**5** are isostructural, therefore the structure of complex **1** determined by the single crystal X-ray diffraction data is discussed in detail as the representative.

Structural description of complex 1

The asymmetric unit of complex **1** is composed of two Eu(III) atoms, two O atoms, one OH group, three ligands (each contributing two oxygen atoms) and one water molecule with the formula of $[Eu_2(\mu_3\text{-}O)_2(OH)(HQXD)(H_2QXD)_2]\cdot H_2O$ (Fig. 2).

Among the three ligands, two present as H_2QXD, *i.e.,* in its neutral form (I) while the third one is in an anion form HQXD$^-$ (II), that is, it dissociates a proton. The O–C bond lengths of the three ligands fall in the range of 1.226(1) to 1.319(1) Å while the N–C bond lengths vary from 1.262(2) to 1.323(1) Å, which reflect the resonance effects in the conjugated systems of N=C–O and N–C=O (Table S1†). The very short N4–C10 (1.262 (1) Å) bond supports the removal of proton from the N4 atom and the formation of strong double bond interactions between N4 and C10. There are total ten oxygen atoms (O1–O10) in asymmetric unit of complex **1** as shown in Fig. 2. The six oxygen atoms (O1–O6) from three ligands adopt different coordination modes: O1, O4 and O6 are μ_2-O atoms that joint to both Eu1 and Eu2 while O2, O3 and O5 atoms are mono-connected, that is, O2 and O5

Table 2 Lattice parameters obtained from Rietveld refinement of powder X-ray diffraction data of complexes **1**–**5**

Sample	Ionic radii	a (Å)	b (Å)	c (Å)	β (°)	V (Å^3)
3 Sm	1.079	7.4241(9)	25.735(3)	13.286(2)	100.008(8)	2499.8(5)
1 Eu	1.066	7.4223(7)	25.736(2)	13.2843(12)	100.008(5)	2498.9(4)
2 Tb	1.040	7.4191(17)	25.727(7)	13.286(4)	99.96(2)	2497.7(11)
4 Dy	1.027	7.4187(6)	25.7331(15)	13.2792(8)	99.950(6)	2497.0(3)

© 2021 The Author(s). Published by the Royal Society of Chemistry

Open Access Article. Published on 29 October 2021. Downloaded on 1/21/2026 12:04:46 AM.
This article is licensed under a Creative Commons Attribution-NonCommercial 3.0 Unported Licence.

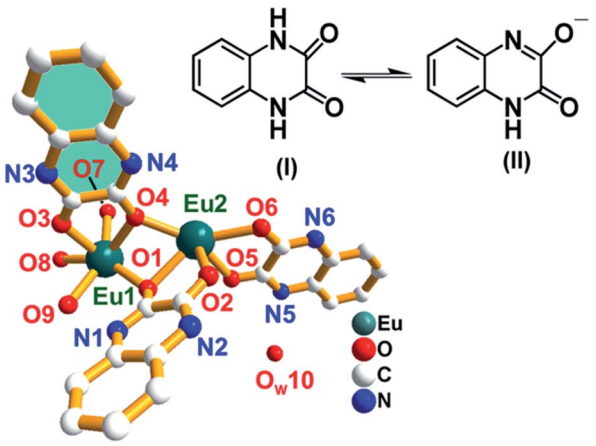

Fig. 2 The asymmetry unit of complex **1** $[Eu_2O_2(OH)(HQXD)(H_2QXD)_2]\cdot H_2O$ with isomeric forms of the ligand. The H atoms are omitted for clarity. Color code: green-blue, Eu; blue, N; red, O; white, C.

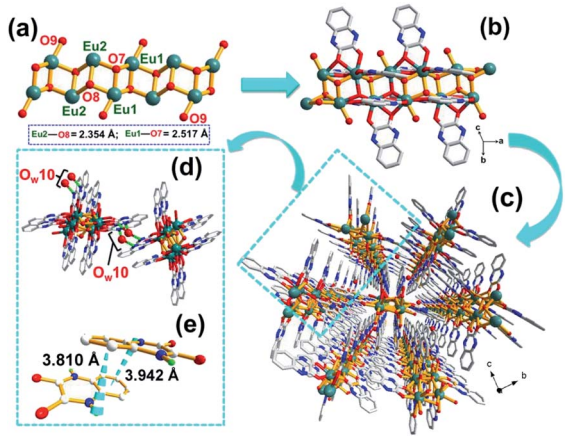

Fig. 3 Structure depiction of complex **1**: (a) "Eu_2O_3" backbone of the 1D chiral chain; (b) 1D chiral chains along the *a*-direction; (c) formation of 3D supramolecular network by hydrogen bonding and π···π interactions of the ligands; (d) hydrogen bonding interactions between water molecules and ligands; (e) π···π interactions between the ligands. Color code: green-blue, Eu; blue, N; red, O; white, C; green, H.

only connected to Eu2 and O3 to Eu1. It means that the two O atoms of each ligand show two kinds of coordination modes: one is mono-connected and the other is bi-connected, as shown in Fig. 2. The two oxygen atoms (O7 and O8) are tri-connected atoms and represented as μ_3-O atoms. O7 is connected to two Eu1 and one Eu2 atoms. O8 is connected to two Eu2 and one Eu1 atoms. The μ_3-O atoms (O7 and O8) are connected to Eu1 and Eu2 atoms giving rise to a zigzag infinite 1D chiral chain, and an additional O9 atom is linked to Eu1 as terminal OH group, as shown in Fig. 3a. Water (O_W10) resides as uncoordinated molecule in the structure. Fig. 3b shows 1D chiral chain along *a*-direction. Thus Eu1 and Eu2 are eight coordinated in the complex **1**. The eight Eu–O bond distances for Eu1 and Eu2 are given in Table S1 in ESI.† The coordination environment around Eu(III) in complex **1** is shown in Fig. S2.†

The six oxygen atoms (O1–O6) from three ligands adopt different coordination modes: O1, O4 and O6 are μ_2-O atoms that joint to both Eu1 and Eu2 while O2, O3 and O5 atoms are mono-connected, that is, O2 and O5 only connected to Eu2 and O3 to Eu1. Water (O_W10) resides as uncoordinated molecule in the structure. It means that the two O atoms of each ligand show two kinds of coordination modes: one is mono-connected and the other is bi-connected, as shown in Fig. 3b. The Eu–O bond distances are in the range of 2.322–2.572 Å and the O–Eu–O bond angles varies from 71.8(2)° to 157.3(2)°, which are consistent with the distorted cubic environments around Eu atoms (Table S1†). The 1D chiral chains are well organized in an ordered manner along the *a*-direction, forming the 3D structure (Fig. 3c). The hydrogen bonding interactions between the uncoordinated water molecules and ligands by O···H···N interactions N1–H(1A)···O9 (2.71 Å), N2–H(2A)···O10 (2.83 Å), N4–H(4A)···O8 (2.89 Å), N5–H(5A)···O(10) (2.79 Å), and N6–H(6A)···O7 (2.78 Å) to stabilize the arrangement (Fig. 3d and Table S2†). This distribution also highlights the existence of π···π stacking interactions of benzyl rings between adjacent ligands and more O/N/C–H···π offset interactions (N5–H5A = 3.810 Å, N2–H2A = 3.942 Å) among hydropyrazine rings, as shown in Fig. 3e.

Thermal, FT-IR and UV-Vis spectroscopic analysis

The thermal stabilities of all complexes **1–5** are similar in the temperature range from 25 to 800 °C under argon at a heating rate of 10 °C min^{-1}. The complexes **1–5** are decomposed in two steps (Fig. S3†). The initial mass loss 2.52%, 2.12%, 2.02%, 2.18% and 2.03% (calcd, 2.10%, 2.07%, 2.11%, 2.05% and 2.07% respectively) between 80 °C to 140 °C corresponds to the departure of the water molecule with remaining structure. The change above 300 °C reveals the decomposition of the complexes, and the total weight loss of the complexes (59.51% for **1**, 58.89% for **2**, 59.90% for **3** 58.19% for **4** and 58.97% for **5**) corresponds to the destruction of the three organic ligands (*i.e.*, $C_8N_2O_2H_6$) and hydroxyl groups (calcd, 60.02% for **1**, 59.03% for **2**, 60.24% for **3**, 58.55% for **4** and 59.17% for **5**). The total calculated weight losses, (62.12% for **1**, 61.1% for **2**, 62.35% for **3**, 60.6% for **4** and 61% for **5**), are well matched with the experimental results (62.03% for **1**, 61.01% for **2**, 61.92% for **3**,

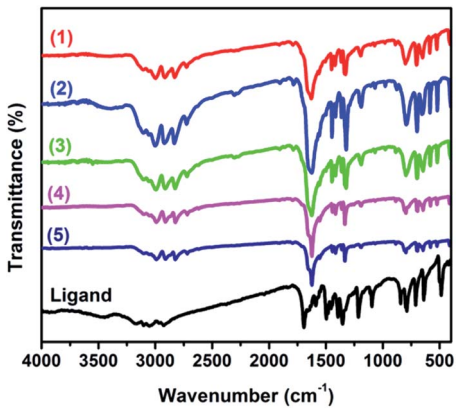

Fig. 4 FT-IR spectra of H_2QXD and complexes **1–5**.

© 2021 The Author(s). Published by the Royal Society of Chemistry

Open Access Article. Published on 29 October 2021. Downloaded on 1/21/2026 12:04:46 AM. This article is licensed under a Creative Commons Attribution-NonCommercial 3.0 Unported Licence.

60.37% for **4** and 61.24% for **5**). All the complexes show three endothermic peaks as shown in Fig. S3.† The first one relates to the removal of water molecules while second and the third peaks correspond to the decomposition of the ligands.

FT-IR spectra of free H_2QXD and complexes **1–5** are shown in Fig. 4. The FT-IR spectrum of H_2QXD shows strong absorption band at 1700 cm^{-1} which is assigned to the stretching vibration of the carbonyl group ν(C=O).[12] The weak intensity bands at 3254 and 3279 cm^{-1} can be assigned to the aromatic ν(N–H) stretching and the peaks at 848 and 786 cm^{-1} and (3000–3100) are assigned to the aromatic C–H bonds.[19] The bands in the region of 1595–1501 cm^{-1} are attributed to aromatic ν(C=C).[19,20] The FT-IR spectra of all complexes **1–5** are similar. The characteristic frequencies of ν(C=O) at of 1700 cm^{-1} in the free ligand shifts to 1628, 1624, 1631 1629 cm^{-1} and 1630 in complexes **1** to **5** respectively, indicating that the oxygen atoms from carbonyl group of the ligands are involved in coordination interaction with Ln(III). The UV-Vis absorption spectrum of H_2QXD in ethanol and water is depicted in Fig. S4† and absorption maxima is given in Table S3.† The ligand (H_2QXD) was found to be insoluble in the non-polar solvents. However, red shift was observed with the increasing polarity of the solvents. In the current case, (where the H_2QXD is viewed as the dione, the two carbonyl groups, joined to a rigid structure, will be *cis* to each other) the ligand can have four n → π* transitions, two of them are forbidden. The data of ε values (Table S3†) clearly indicated that the long wavelength band of H_2QXD was of π → π* character and the n → π* transitions which were substantially blue shifted are hidden under the strong π → π* transitions.[21] The absorption spectrum of H_2QXD has been studied at different pH values. The absorption spectrum of H_2QXD is red shifted on increasing the alkalinity of the solution and there are no spectra changes are found after pH 12. This indicates that anionic species are formed in this case.[21] Molar extinction coefficient value at 236 nm is 2.29×10^3 $mmol^{-1}$ cm^{-1}, indicating the ligand being an adequate light-harvesting chromophore for the sensitization of lanthanide luminescence (Fig. S4†). The singlet energy level of H_2QXD ligand (^{1}s, 36 101 cm^{-1} (277 nm)) was also calculated from UV-Vis absorption spectrum absorbance edge of H_2QXD.

Diffuse reflectance spectroscopy

The diffuse reflectance spectra of complexes **1–5** and free ligand H_2QXD are shown in Fig. S5.† The free ligand displays an absorption band in the UV region at 378–420 nm, which is assigned to n → π* transition.[21] The spectra of **1–5** are similar to the one observed for the free ligand, implying that the singlet excited state of the free ligand is not significantly affected by the complexation of the Ln^{3+} ion. Therefore the observed band in the UV region of **1–5** and of the H_2QXD can be assigned to electronic transitions from the ground state level S_0 to the excited level S_1 of H_2QXD. Additionally, a small red shift that is discernible in the absorption maximum of the complexes is attributable to an effective interaction between the lanthanide cations and the organic ligand.[22]

Phosphorescence spectrum studies

In order to determine the triplet energy levels of lanthanide complexes, it is common practice to use analogous of a non-emitting lanthanide ion (*i.e.*, La^{3+}, Gd^{3+}, and Lu^{3+}) because there is no f–f transitions for such lanthanides.[23] In the case of Gd^{3+} ion, lowest excited state $^6P_{7/2}$ is too high to accept energy from a ligand, the triplet energy level of the corresponding ligand can be obtained from the phosphorescence spectrum of its Gd^{3+} complex (which is synthesized for the sake of measurement) at 77 K.[24] Tangent method is applied to phosphorescence spectrum of complex **5** to determine the triplet energy level ($^3\pi\pi^*$). As shown in Fig. S6,† in the phosphorescence spectrum of complex **5**, the *x* intercept is observed at 402 nm which is related to the triplet energy level ($^3\pi\pi^*$) at 24 875 cm^{-1}.

Energy transfer mechanism

Reinhoudt's empirical rule states that when ΔE ($^1\pi\pi^*$–$^3\pi\pi^*$) of a ligand is at least 5000 cm^{-1} then the intersystem crossing (ISC) process becomes effective.[25] The calculated singlet state energy level ($^1\pi\pi^*$) of H_2QXD was 36 101 cm^{-1} (277 nm) based on the UV-Vis spectrum of H_2QXD. Since the lowest excited state $^6P_{7/2}$ of Gd^{3+} ion is too high to accept energy from a ligand, the data obtained from the phosphorescence spectrum of the complex actually reveal the triplet energy level of the corresponding ligand.[24] So the calculated triplet state energy ($^3\pi\pi^*$) level at 24 875 cm^{-1} (402 nm) is due to the H_2QXD ligand. Therefore the energy gap between the $^1\pi\pi^*$ and $^3\pi\pi^*$ level is 11 226 cm^{-1} for H_2QXD, indicating that the intersystem crossing process in the title complexes is effective as shown in Table 3. According to the Latva intramolecular energy transfer mechanism,[26] the energy difference between the lowest triplet level of a ligand and the resonant energy level of the Ln^{3+} ion plays a key role in the energy transfer process in Ln-complexes. The energy differences for the Eu^{3+} and Tb^{3+} ions fall in the range of 3000 ± 500 cm^{-1} and 3500 ± 1000 cm^{-1} respectively.[27] The photoluminescence intensities of the lanthanide complexes will decrease when the values of energy difference fall in out of the range.[28] As listed in Table 3, the energy difference between the lowest triplet levels of the H_2QXD ligand and the resonant energy levels of the Eu^{3+} ($^5D_1$, 19 026 cm^{-1}), Tb^{3+} ($^5D_4$, 20 500 cm^{-1}), Sm^{3+} ($^4G_{5/2}$, 17 900 cm^{-1}) and Dy^{3+} ions ($^4F_{9/2}$, 20 875 cm^{-1}) are 5849 cm^{-1}, 4375 cm^{-1}, 6975cm^{-1}, and 4000 cm^{-1} respectively.[29,30] The resonant energy level of Tb^{3+} is within the optimal energy gap implying that the H_2QXD is more suitable sensitizer for luminescence of Tb^{3+} ions rather than Eu^{3+}, Sm^{3+} and Tb^{3+} ions. Thus, among the complexes **1–5**, it is predicted that complex **2** can emit strong green characteristic luminescence of Tb^{3+} ions. The schematic energy level diagram and the energy transfer process in complexes **1–5** are shown in Fig. 5.

Photo-luminescence properties of complexes 1 and 2

The complex **1** in solid state emits characteristic red light under UV light irradiation. The corresponding excitation and emission spectra of complex **1** are shown in Fig. 6a. The strong

Open Access Article. Published on 29 October 2021. Downloaded on 1/21/2026 12:04:46 AM.
This article is licensed under a Creative Commons Attribution-NonCommercial 3.0 Unported Licence.

Table 3 The singlet ($^1\pi\pi^*$) and triplet ($^3\pi\pi^*$) energy levels of the H_2QXD ligand and energy level differences between Ln^{3+} ions and the H_2QXD ligand in the complexes **1–4**

Ligand	$^1\pi\pi^*$ (cm^{-1})	$^3\pi\pi$ (cm^{-1})	ΔE ($^1\pi\pi^*$–$^3\pi\pi^*$)	ΔE ($^3\pi\pi^*$–$^5D_1$)	ΔE ($^3\pi\pi^*$–$^5D_4$)	ΔE ($^3\pi\pi^*$–$^4G_{5/2}$)	ΔE ($^3\pi\pi^*$–$^4F_{9/2}$)
H_2QXD	36 101 cm^{-1}	24 875 cm^{-1}	11 226 cm^{-1}	5849 cm^{-1}	4375 cm^{-1}	6975 cm^{-1}	4000 cm^{-1}

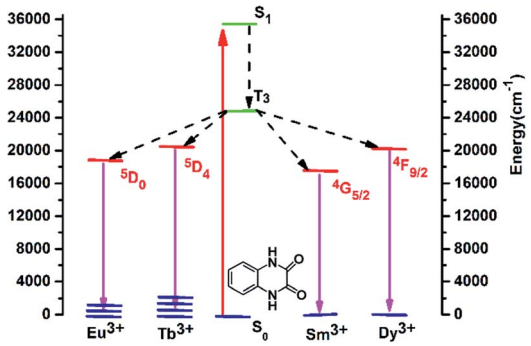

Fig. 5 Schematic energy level diagram and the energy transfer process in complexes **1–4**.

absorption broad band in the region 200–350 nm centered at 270 nm is ascribed to the electronic transitions of the ligand, and the peaks at 390, 414 and 464 nm can be assigned to the $^7F_0 \rightarrow {}^5L_6$, $^7F_0 \rightarrow {}^5D_3$ and $^7F_0 \rightarrow {}^5D_2$ transitions of Eu(III). The emission spectrum of **1** under 270 nm excitation wavelength corresponds to the typical $^5D_0 \rightarrow {}^7F_J$ ($J = 1, 2, 3, 4$) transitions of Eu(III), showing the energy transfer from ligand to Eu(III). The peaks at 592 nm relates to the magnetic dipole transition of $^5D_0 \rightarrow {}^7F_1$, while the peak of 615 nm corresponds to electric dipole transition of $^5D_0 \rightarrow {}^7F_2$. The former is independent from the coordination sphere, but the later is sensitive to the coordination environment. The asymmetric environment around the metal ion can cause the enhancement of the intensity.[12,31–34] Complex **1** shows intense red colour and the intensity ratio of 615 to 592 nm indicates that Eu^{3+} ion has an asymmetric coordination sphere, which is consistent with the structure analysis. The asymmetric coordination environment around Eu(III) in complex **1** is shown in Fig. S2.† The other two weak emission peaks at 653 nm and 700 nm correspond to the $^5D_0 \rightarrow {}^7F_3$ and $^5D_0 \rightarrow {}^7F_4$ transition respectively.[35]

Complex **2** emits green light under UV lamp, and its excitation and emission spectra in the solid state is shown in Fig. 6b. The broad and strong excitation spectrum with three peaks at 230, 268 and 302 nm by detecting emission peak of 546 nm is an overlap of the absorption of the ligands (Fig. S4†) and $O^{2-} \rightarrow Eu^{3+}$ charge transfer, which also indicates the energy transfer from the ligand to the metal center.[24] The four emission peaks are characteristic $^5D_4 \rightarrow {}^7F_J$ ($J = 6, 5, 4, 3$) transitions of the Tb(III).[12,19,36] The strongest peak at 546 nm corresponds to $^5D_4 \rightarrow {}^7F_5$ emission, and the weakest peak at 610 nm corresponds to $^5D_4 \rightarrow {}^7F_6$ transition of Tb(III). The photo-luminescent properties of complex **3** and **4** in the solid state are given in ESI (Fig. S7†).

Lift time decay and quantum yield

The room temperature decay curve $^5D_0$ (Eu^{3+}) of complex **1** in solid state was monitored within the more intense peak of $^5D_0 \rightarrow {}^7F_2$ (615 nm) when excited at 270 nm. The emission decay curve of complexes **1** at room temperature (Fig. 7) is well fitted by a mono-exponential function. The lifetime decays values of **1** (0.99 ms).[37] The sensitization pathway in a luminesescent for Ln-complexes is well explained by the photophysical mode. The overall quantum yield (Φ_{tot}) of ligand-sensitized Ln-emission is calculated by using the following formula:[38]

$$\Phi_{tot} = \eta_{sens}\Phi_{Ln} \quad (1)$$

where η_{sens} is the ligand sensitization efficiency and Φ_{Ln} shows the intrinsic quantum yield of the lanthanide luminescence. The η_{sens} is the product of the two processes involving inter-system crossing (ISC) from the first excited singlet state of the ligand to the triplet state and energy transfer to the lanthanide. The intrinsic quantum yield of the lanthanide luminescence step (Φ_{Ln}) can be calculated on the basis of observed luminescence lifetime (τ_{obs}) and radiative lifetime (τ_R) of the Eu(III) $^5D_0 \rightarrow {}^7F_1$ transitions by using:[39]

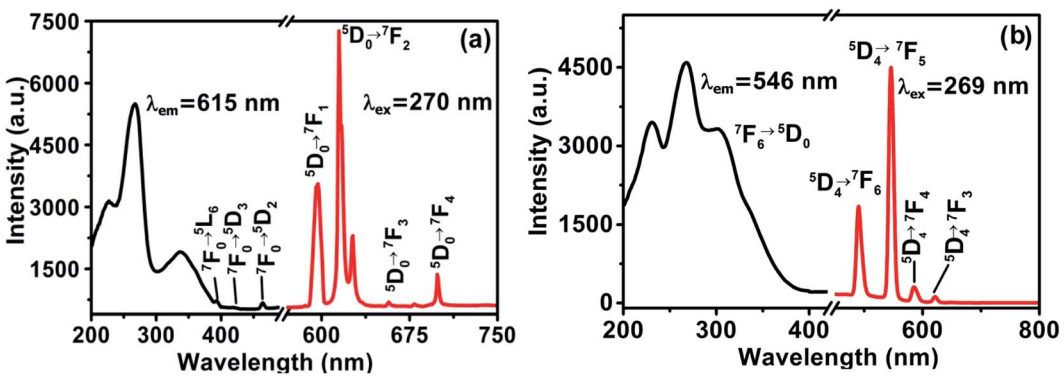

Fig. 6 Excitation and emission spectra: (a) $[Eu_2O_2(OH)(HQXD)(H_2QXD)_2]\cdot H_2O$ (**1**), (b) $[Tb_2O_2(OH)(HQXD)(H_2QXD)_2]\cdot H_2O$ (**2**).

© 2021 The Author(s). Published by the Royal Society of Chemistry

Open Access Article. Published on 29 October 2021. Downloaded on 1/21/2026 12:04:46 AM.
This article is licensed under a Creative Commons Attribution-NonCommercial 3.0 Unported Licence.

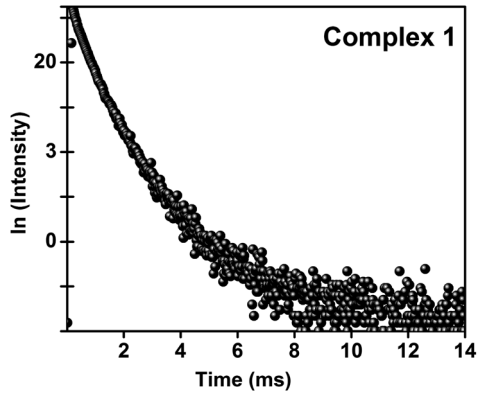

Fig. 7 Room temperature emission decay curve of **1** excited at 270 nm and monitored at 615 nm.

$$\Phi_{Ln} = \tau_{obs}/\tau_R \quad (2)$$

$$1/\tau_R = A_{MD,0} n^3 (I_{tot}/I_{MD}) \quad (3)$$

where $A_{MD,0} = 14.65\ s^{-1}$ is the spontaneous emission probability of the $^5D_0 \rightarrow {}^7F_1$ transition of Eu(III), n, the refractive index of the medium, I_{tot}/I_{MD}, the ratio of the integrated total area of the corrected Eu(III) emission spectrum to the area of magnetic dipole $^5D_0 \rightarrow {}^7F_1$ transition. Overall quantum yield (Φ_{tot}) was determined as 3.94%. By using eqn (1)–(3); radiative lifetime (τ_R), experimentally determined luminescence lifetime (τ_{obs}) intrinsic quantum yield (Φ_{Ln}), and sensitization efficiency (η_{sens}) values were calculated as 6.97 ms, 0.99 ms, 14.20%, and 27.74% respectively.

Photo-luminescence (Pl) based sensing ability of the complex 2′

Complex **2** was heated at 150 °C for 12 hours to remove the uncoordinated water molecule and the anhydrous complex **2′** was obtained for the investigation of the sensing effect by small molecules. The comparative powder X-ray diffraction patterns of complexes **2** and **2′** indicate that the removal of the water molecules did not cause the change the main structure, as shown in Fig. S8.† The FT-IR spectrum of complex **2′** is much similar to complex **2** as shown in Fig. S9.† This reveals that the removal of water molecule did not affect the major peaks in FT-IR spectrum of complex **2′**. The removal of on water molecule is evident from the thermal analysis of complexes **2′**. As shown in FigAs shown in Fig. S10† There is not initial mass loss between 80 °C to 140 °C corresponding to the departure of the water molecule with remaining structure in complex **2′**. The change above 300 °C reveals the decomposition of the complex **2′**, and the weight loss of the complex **2′** (58.56%) corresponds to the destruction of the three organic ligands (*i.e.*, $C_8N_2O_2H_6$) and hydroxyl groups (calcd., 58.96% for **2′**). No endothermic peak relating to the removal of water molecule was observed. The solvent emulsions were prepared by mixing 2.00 mg of samples with 4.00 mL of each solvent (tertiary butanol (*t*-butynol), secondary butanol, *n*-butanol, isopropyl alcohol (IPA), propanol, ethanol (EtOH), methanol (MeOH), H_2O, DMSO, DMF, $CHCl_3$, and THF separately). The powder was filtered off after aging of two days and the luminescent spectra were measured at excitation wavelength of 270 nm. The peak at 546 nm ($^5D_4 \rightarrow {}^7F_5$ transition) was selected for further PL study (Fig. 8).

It is found that the luminescent property of complex **2′** is greatly dependent on the identity of the solvents.[40] Tertiary-butanol has the strongest sensitizing effect and THF shows significant quenching influence on the luminescence intensity of **2′**, in which luminescence almost disappeared when complex **2′** was immersed in pure THF. Complex **2′** exhibits varying degrees of increasing or quenching effects by other solvents. Such solvent-dependent luminescence properties are very interesting and important for the selective sensing of *t*-butanol or THF solvent molecules (Fig. 8). Although the mechanism for such enhancing and quenching effects is still not very clear, it has been found that when lanthanide–organic frameworks

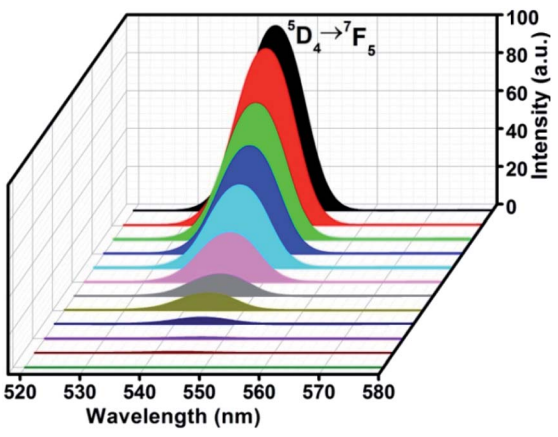

Fig. 8 The emission spectra of complex **2′** at excitation wavelength λ_{ex} = 270 nm after treated by different solvents. Colour codes: *t*-butanol, black; secondary butanol, red; *n*-butanol, green; IPA, blue; propanol, cyan; ethanol, magenta; methanol, gray; water, dark yellow; DMSO, navy blue; DMF, violet; $CHCl_3$, wine; and THF, olive.

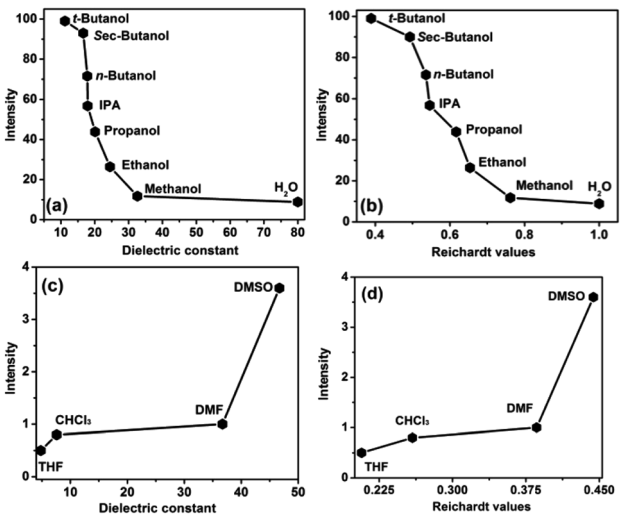

Fig. 9 Photo-luminescence intensities of complex **2′** with respect to the dielectric constant and Reichardt values of solvents. (a) and (b) Show the effect of hydroxylic solvents; (c) and (d) present the effect of nonhydroxylic solvents.

Open Access Article. Published on 29 October 2021. Downloaded on 1/21/2026 12:04:46 AM.
This article is licensed under a Creative Commons Attribution-NonCommercial 3.0 Unported Licence.

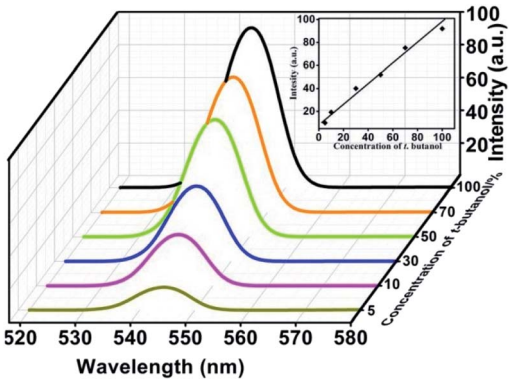

Fig. 10 The emission spectra of complex 2′ with different concentrations of *t*-butanol (λ_{ex} = 270 nm). Inset shows the linear fluorescence enhancement *vs.* *t*-butanol concentration.

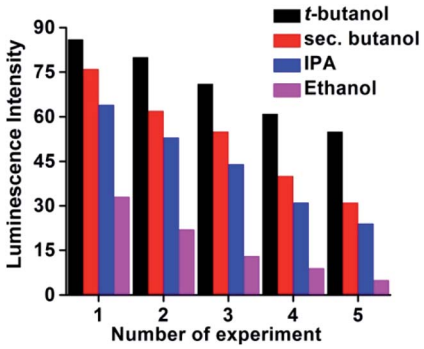

Fig. 11 Reusability of the complex 2′ in *t*-butanol, *sec*-butanol, IPA, and ethanol (λ_{ex} = 270 nm).

interact with polar solvents, intermolecular hydrogen bonds always form between solvent molecules and lanthanide complexes.[12,41] These hydrogen bonds could change the solute and solvent electronic coupling which then greatly affect the luminescent properties of lanthanide complexes.[42]

In order to understand the solvent effect toward complex 2′, the photo-luminescent intensities of complex 2′ were plotted against the dielectric constants and normalized Christian Reichardt values of the solvents as shown in Fig. 9. The corresponding data of the solvents are listed in Table S4 in ESI.†[43,44] The twelve solvents can be divided into two groups: hydroxylic solvents (*t*-butanol, *sec*-butanol, *n*-butanol, IPA, propanol, EtOH, MeOH, H_2O) and the nonhydroxylic solvents (DMSO, DMF, $CHCl_3$, THF). It can be seen that PL intensity of complex 2′ decreases with the increase of dielectric constant and E_T^N values for hydroxylic solvents (Fig. 9a and b), while PL intensity increases with the increase of dielectric constant and E_T^N for nonhydroxylic solvents (Fig. 9c and d).[43]

Since *t*-butanol shows an enhancing effect on the PL intensity of complex 2′, it was selected for further study. Water was selected as a comparison solvent in the treatment of complex 2′. Complex 2′ was dispersed in H_2O, and different volume of *t*-butanol was added into the aqueous emulsion, while the concentration of Tb(III) was kept constant. As shown in Fig. 10, as the *t*-butanol concentration was increased (5%, 10%, 30%, 50%, 70% and 100%), the intensity of complex 2′ gradually increased with increasing the concentration of *t*-butanol, and was nearly proportional to the *t*-butanol concentration (Fig. 10).

Reusability study of complex 2′

Additionally the reusability of the complex 2′ was also tested by taking *t*-butanol, *sec*-butanol, IPA, and EtOH as examples. We explored the sensing ability of the complex 2′ by filtering off the dispersed solution after use. The filtrate was washed several times with H_2O/EtOH and dried under vacuum for 12 h. It is noteworthy (Fig. 11) that complex 2′ almost regains its initial fluorescence intensity, implying a high photo-stability of the material for a long time without any contamination.

Conclusions

Five isostructural lanthanide complexes $[Ln_2O_2(OH)(HQXD)(H_2QXD)_2]\cdot H_2O$ (Ln = Eu, Tb, Sm Dy and Gd; H_2QXD = quinoxaline-2,3(1*H*,4*H*)-dione) were obtained by hydrothermal method. The structure of the complexes features in 1D chiral "Ln_2O_3" chains which are surrounded by the organic ligands and further organized *via* hydrogen bonds and offset stacking ($\pi\cdots\pi$) interactions to form the 3D supramolecular frameworks. Among the three ligands, two present as their neutral form (H_2QXD) and one losses a proton and appears as an anion ($HQXD^-$). The two oxygen atoms of each ligand adopt different coordination modes: one links two Eu atoms, and the other bonds only to a single Eu cation. These new complexes exhibit characteristic luminescent emissions of the corresponding lanthanide cations, and present efficient energy transfer from the ligands which act as antenna to absorb the photo-excitation energy. The energy transfer mechanism investigations show that the energy transition from the triplet energy level ($3\pi\pi^*$) of ligand H_2QXD to Tb^{3+} cation is more effective than that of Eu^{3+}, Dy^{3+} Sm^{3+} and Gd^{3+} ions. The sensing studies of Tb(III) complex 2′ by small molecules reveal that the nature of the solvents play key role in the enhancing or quenching the photo-luminescence of the complex. It was found that *t*-butanol is an excellent sensitizer while tetrahydrofuran (THF) is highly quenching species. The complex 2′ regained almost 70% of its first photo-luminescent intensity after 5 cycles, revealing a prospect for its reusability.

Author contributions

The manuscript was written through contributions of all authors. All authors have given approval to the final version of the manuscript.

Conflicts of interest

There are no conflicts to declare.

Acknowledgements

This project was financially supported by the National Natural Science Foundation of China (11275012).

© 2021 The Author(s). Published by the Royal Society of Chemistry

Open Access Article. Published on 29 October 2021. Downloaded on 1/21/2026 12:04:46 AM. This article is licensed under a Creative Commons Attribution-NonCommercial 3.0 Unported Licence.

References

1 S.-R. Zhang, D.-Y. Du, J.-S. Qin, S.-L. Li, W.-W. He, Y.-Q. Lan and Z.-M. Su, 2D Cd(II)-lanthanide(III) heterometallic-organic frameworks based on metalloligands for tunable luminescence and highly selective, sensitive, and recyclable detection of nitrobenzene, *Inorg. Chem.*, 2014, **53**, 8105–8113.

2 Y. Lü, W. Zhan, Y. He, Y. Wang, X. Kong, Q. Kuang, Z. Xie and L. Zheng, MOF-Templated Synthesis of Porous Co3O4 Concave Nanocubes with High Specific Surface Area and Their Gas Sensing Properties, *ACS Appl. Mater. Interfaces*, 2014, **6**, 4186–4195.

3 B. Chen, Y. Yang, F. Zapata, G. Lin, G. Qian and E. B. Lobkovsky, Luminescent open metal sites within a metal–organic framework for sensing small molecules, *Adv. Mater.*, 2007, **19**, 1693–1696.

4 E. Y. Lee, S. Y. Jang and M. P. Suh, Multifunctionality and Crystal Dynamics of a Highly Stable, Porous Metal–Organic Framework [Zn4O(NTB)2], *J. Am. Chem. Soc.*, 2005, **127**, 6374–6381.

5 L. E. Kreno, K. Leong, O. K. Farha, M. Allendorf, R. P. Van Duyne and J. T. Hupp, Metal–Organic Framework Materials as Chemical Sensors, *Chem. Rev.*, 2012, **112**, 1105–1125.

6 Y. Cui, B. Chen and G. Qian, Lanthanide metal-organic frameworks for luminescent sensing and light-emitting applications, *Coord. Chem. Rev.*, 2014, **273**, 76–86.

7 y. J. Kuppler, D. J. Timmons, Q. Fang, J. Li, T. A. Makal, D. Young, D. Yuan, D. Zhao, W. Zhuang and H. Zhou, 2009.

8 G. Muller, Luminescent chiral lanthanide (III) complexes as potential molecular probes, *Dalton Trans.*, 2009, 9692–9707.

9 G. R. Desiraju, Designer crystals: intermolecular interactions, network structures and supramolecular synthons, *Chem. Commun.*, 1997, 1475–1482.

10 H.-L. Jiang, Y. Tatsu, Z.-H. Lu and Q. Xu, Non-, micro-, and mesoporous metal–organic framework isomers: reversible transformation, fluorescence sensing, and large molecule separation, *J. Am. Chem. Soc.*, 2010, **132**, 5586–5587.

11 J.-M. Zhou, W. Shi, N. Xu and P. Cheng, Highly selective luminescent sensing of fluoride and organic small-molecule pollutants based on novel lanthanide metal–organic frameworks, *Inorg. Chem.*, 2013, **52**, 8082–8090.

12 W. Ahmad, L. Zhang and Y. Zhou, 2-D lanthanide–organic complexes constructed from 6, 7-dihydropyrido (2, 3-d) pyridazine-5, 8-dione: synthesis, characterization and photoluminescence for sensing small molecules, *CrystEngComm*, 2014, **16**, 3521–3531.

13 J.-C. G. Bünzli and S. V. Eliseeva, Intriguing aspects of lanthanide luminescence, *Chem. Sci.*, 2013, **4**, 1939–1949.

14 N. Sabbatini, M. Guardigli and J.-M. Lehn, Luminescent lanthanide complexes as photochemical supramolecular devices, *Coord. Chem. Rev.*, 1993, **123**, 201–228.

15 G. Kaupp and M. R. Naimi-Jamal, Quantitative cascade condensations between o-phenylenediamines and 1,2-dicarbonyl compounds without production of wastes, *Eur. J. Org. Chem.*, 2002, **2002**, 1368–1373.

16 H. M. Rietveld, A profile refinement method for nuclear and magnetic structures, *J. Appl. Crystallogr.*, 1969, **2**, 65–71.

17 G. Sheldrick, *SHELXTL V5. 1 software reference manual*, Bruker AXS Inc., Madison, Wisconsin, USA, 1997.

18 G. M. Sheldrick, Program for crystal-structure refinement, *SHELX-97*, 1997.

19 W. Ahmad, L. Zhang and Y. Zhou, A series of mononuclear lanthanide complexes featuring 3-D supramolecular networks: synthesis, characterization and luminescent properties for sensing guest molecules, *Photochem. Photobiol. Sci.*, 2014, **13**, 660–670.

20 A. Şengül and H. Arslan, Synthesis and Characterization of Novel Polyamide and Polyhydrazides Based on the 6, 6-disubstituted-2, 2-bipyridine, *Turk. J. Chem.*, 2008, **32**, 355–364.

21 M. Krishnamurthy, K. A. Iyer and S. K. Dogra, Electronic structure of quinoxaline-2, 3 (1H, 4H) dione and its prototropic species in the ground and excited singlet states, *J. Photochem.*, 1987, **38**, 277–287.

22 L. F. Marques, M. V. dos Santos, S. J. Ribeiro, E. E. Castellano and F. C. Machado, Terbium (III) and dysprosium (III) 8-connected 3D networks containing 2, 5-thiophenedicarboxylate anion: crystal structures and photoluminescence studies, *Polyhedron*, 2012, **38**, 149–156.

23 M. D. Regulacio, M. H. Pablico, J. A. Vasquez, P. N. Myers, S. Gentry, M. Prushan, S.-W. Tam-Chang and S. L. Stoll, Luminescence of Ln (III) dithiocarbamate complexes (Ln= La, Pr, Sm, Eu, Gd, Tb, Dy), *Inorg. Chem.*, 2008, **47**, 1512–1523.

24 P. C. Soares-Santos, L. Cunha-Silva, F. A. A. Paz, R. A. Ferreira, J. Rocha, L. D. Carlos and H. I. Nogueira, Photoluminescent lanthanide-organic bilayer networks with 2, 3-pyrazinedicarboxylate and oxalate, *Inorg. Chem.*, 2010, **49**, 3428–3440.

25 F. J. Steemers, W. Verboom, D. N. Reinhoudt, E. B. van der Tol and J. W. Verhoeven, New sensitizer-modified calix [4] arenes enabling near-UV excitation of complexed luminescent lanthanide ions, *J. Am. Chem. Soc.*, 1995, **117**, 9408–9414.

26 M. Latva, H. Takalo, V.-M. Mukkala, C. Matachescu, J. C. Rodríguez-Ubis and J. Kankare, Correlation between the lowest triplet state energy level of the ligand and lanthanide (III) luminescence quantum yield, *J. Lumin.*, 1997, **75**, 149–169.

27 M. Kleinerman, Energy migration in lanthanide chelates, *J. Chem. Phys.*, 1969, **51**, 2370–2381.

28 Y. Gai, F. Jiang, L. Chen, M. Wu, K. Su, J. Pan, X. Wan and M. Hong, Europium and terbium coordination polymers assembled from hexacarboxylate ligands: structures and luminescent properties, *Cryst. Growth Des.*, 2014, **14**, 1010–1017.

29 W. Carnall, P. Fields and K. Rajnak, Spectral intensities of the trivalent lanthanides and actinides in solution. II. Pm3+, Sm3+, Eu3+, Gd3+, Tb3+, Dy3+, and Ho3+, *J. Chem. Phys.*, 1968, **49**, 4412–4423.

30 W. Carnall, P. Fields and K. Rajnak, Electronic energy levels of the trivalent lanthanide aquo ions. III. Tb3+, *J. Chem. Phys.*, 1968, **49**, 4447–4449.

Open Access Article. Published on 29 October 2021. Downloaded on 1/21/2026 12:04:46 AM.
This article is licensed under a Creative Commons Attribution-NonCommercial 3.0 Unported Licence.

31 P. C. R. Soares-Santos, L. Cunha-Silva, F. A. A. Paz, R. A. S. Ferreira, J. Rocha, L. D. Carlos and H. I. S. Nogueira, Photoluminescent Lanthanide-Organic Bilayer Networks with 2,3-Pyrazinedicarboxylate and Oxalate, *Inorg. Chem.*, 2010, **49**, 3428–3440.

32 B. Francis, D. A. Raj and M. Reddy, Highly efficient luminescent hybrid materials covalently linking with europium (III) complexes via a novel fluorinated β-diketonate ligand: synthesis, characterization and photophysical properties, *Dalton Trans.*, 2010, **39**, 8084–8092.

33 G. R. Choppin and D. R. Peterman, Applications of lanthanide luminescence spectroscopy to solution studies of coordination chemistry, *Coord. Chem. Rev.*, 1998, **174**, 283–299.

34 Z.-J. Zhang, J.-L. Yuan, X.-J. Wang, D.-B. Xiong, H.-H. Chen, J.-T. Zhao, Y.-B. Fu, Z.-M. Qi, G.-B. Zhang and C.-S. Shi, Luminescence properties of CaZr (PO4) 2: RE (RE= Eu3+, Tb3+, Tm3+) under x-ray and VUV–UV excitation, *J. Phys. D: Appl. Phys.*, 2007, **40**, 1910.

35 Y.-G. Sun, X.-M. Yan, F. Ding, E.-J. Gao, W.-Z. Zhang and F. Verpoort, A novel 3D 4d–4f heterometallic coordination polymer: synthesis, crystal structure and luminescence, *Inorg. Chem. Commun.*, 2008, **11**, 1117–1120.

36 L. Zhang, S. Xu, Y. Zhou, X. Zheng, C. Yu, Z. Shi, S. ul Hassan and C. Chen, Two isomorphous 3-D lanthanide oxalatophosphonate frameworks based on glyphosate: syntheses, crystal structures, and luminescence properties, *CrystEngComm*, 2011, **13**, 6511–6519.

37 P. C. Soares-Santos, L. s. Cunha-Silva, F. A. A. Paz, R. A. S. Ferreira, J. Rocha, T. Trindade, L. D. Carlos and H. I. Nogueira, Photoluminescent 3D Lanthanide–Organic Frameworks with 2, 5-Pyridinedicarboxylic and 1, 4-Phenylenediacetic Acids, *Cryst. Growth Des.*, 2008, **8**, 2505–2516.

38 S. Comby, D. Imbert, A.-S. Chauvin, J.-C. G. Bünzli, L. J. Charbonnière and R. F. Ziessel, Influence of anionic functions on the coordination and photophysical properties of lanthanide (III) complexes with tridentate bipyridines, *Inorg. Chem.*, 2004, **43**, 7369–7379.

39 M. H. Werts, R. T. Jukes and J. W. Verhoeven, The emission spectrum and the radiative lifetime of Eu 3+ in luminescent lanthanide complexes, *Phys. Chem. Chem. Phys.*, 2002, **4**, 1542–1548.

40 R. Díaz-Torres and S. Alvarez, Coordinating ability of anions and solvents towards transition metals and lanthanides, *Dalton Trans.*, 2011, **40**, 10742–10750.

41 S. Zhang, Z. Wang, H. Zhang, Y. Cao, Y. Sun, Y. Chen, C. Huang and X. Yu, Self-assembly of two fluorescent supramolecular frameworks constructed from unsymmetrical benzene tricarboxylate and bipyridine, *Inorg. Chim. Acta*, 2007, **360**, 2704–2710.

42 J. A. Riddick, W. B. Bunger and T. K. Sakano, *Organic solvents: physical properties and methods of purification*, 1986.

43 C. Reichardt, Solvatochromic dyes as solvent polarity indicators, *Chem. Rev.*, 1994, **94**, 2319–2358.

44 G.-J. Zhao and K.-L. Han, Hydrogen bonding in the electronic excited state, *Acc. Chem. Res.*, 2012, **45**, 404–413.

© 2021 The Author(s). Published by the Royal Society of Chemistry